Original Article

miR-4478 Promotes Ferroptosis of Nucleus Pulposus Cells through Targeting SLC7A11 to Induce IVDD

(miR-4478 / SLC7A11 / iron death / intervertebral disc degeneration)

DONGLIANG GONG[1*], LONG JIA[1*], YUHANG WANG[2], CHENGWEI XU[2], XUXING SUN[2], XIAO WU[1], XIAOJUN HAN[1]

[1]Department of Orthopedics, Qingpu Branch of Zhongshan Hospital Affiliated to Fudan University, Shanghai, China
[2]School of Clinical Medicine, Bengbu Medical University, Bengbu, China
[*]Dongliang Gong and Long Jia contributed to this work equally.

Abstract. Nucleus pulposus cells (NPC) are important for the development of intervertebral disc degeneration (IVDD). miR-4478 can aggravate IVDD, but whether it can aggravate IVDD by regulating ferroptosis in NPC remains unclear. The optimal level of ferroptosis activator RSL3 for eliciting ferroptosis in NPC was screened by Western blot and CCK-8 assay. The targeting relationship between miR-4478 and its potential target solute carrier family 7 member 11 (SLC7A11) was explored based on dual luciferase assay. On this basis, IVDD models were constructed. After over-expression or knockdown of miR-4478 or SLC7A11, CCK-8 and calcein-AM/PI assays were employed to evaluate cell damage. Flow cytometry, Western blot and Prussian blue staining were employed to evaluate oxidation and ferroptosis levels, and histopathological staining was applied to evaluate the intervertebral disc tissue injury degree. The optimal concentration of RSL3 was 1 μM. Under these conditions, miR-4478 or SLC7A11 can be effectively over-expressed or knocked down after transfection. Knockdown of miR-4478 can improve the survival rate of NPC, the level of Fe^{2+} ions, improve the pathological damage of intervertebral disc structure, reduce iron deposition in tissues, and significantly reduce expression of reactive oxygen species (ROS) and ferroptosis-related protein. The levels of antioxidant enzymes were significantly increased. When miR-4478 was over-expressed, the above phenomenon was reversed. On this basis, after SLC7A11 was over-expressed, the effect of miR-4478 up-regulation was weakened, and NPC ferroptosis was improved. miR-4478 can target SLC7A11 to promote NPC damage, peroxide accumulation and iron metabolism disorders, leading to ferroptosis, thereby inducing IVDD.

Received December 24, 2024. Accepted March 16, 2025.

This study was funded by Fudan University Affiliated Zhongshan Hospital Qingpu branch Hospital-level Scientific Research Projects (Nos. QYBS2023-02 and QYM2023-07); Bengbu Medical University, Natural Science Foundation (No. 2023byzd198); Shanghai Association of Integrative Chinese and Western Medicine Community Medicine and Health Management Research Topic Research Special Fund Project (No. 2024-43).

Corresponding authors: Xiao Wu, Department of Orthopedics, Qingpu Branch of Zhongshan Hospital Affiliated to Fudan University, No. 1158 East Park Road,Shanghai 201700, China; E-mail: xwuxiao@sina.com; Xiaojun Han; E-mail: hanxiaojun1221@hotmail.com

Abbreviations: ACSL4 – acyl-CoA synthetase long-chain family member 4, COX-2 – cyclooxygenase 2, FTH1 – ferritin heavy chain 1, IVDD – intervertebral disc degeneration, GPX4 – glutathione peroxidase 4, GSH – glutathione, MDA – malondialdehyde, miR-4478 – microRNA 4478, NPC – nucleus pulposus cells, ROS – reactive oxygen species, SLC7A11 – solute carrier family 7 member 11.

Introduction

Intervertebral disc degeneration (IVDD), a degenerative disease, is a common cause of lumbago. It usually occurs as gradual deterioration of the intervertebral disc structure (Cheung et al., 2009), and it is a complex process involving many factors such as stress, inflammation, immunity and genes (Zielinska et al., 2021). The technical methods for clinical treatment of lumbar disc degeneration are limited. Whether it is traction, physiotherapy, anti-inflammatory analgesia and other conservative treatments, or surgery, it is mainly to relieve pain and current symptoms. At present, the clinical treatment cannot completely block the pathological process of lumbar disc degeneration (Xin et al., 2022). Therefore, it is urgent to solve the key mechanism of IVDD in clinical practice to find the key therapeutic targets for re-

versing IVDD. The intervertebral disc comprises a central nucleus pulposus, a surrounding annulus fibrosus, and two cartilage endplates on the upper and lower edges of the cone. As an avascular tissue, the nucleus pulposus is located between the upper and lower adjacent cartilage endplates and is surrounded by annulus fibrosus. The extracellular matrix of nucleus pulposus cells (NPC) contains elastic components such as collagen; they are the main functional ingredients of the intervertebral disc that can withstand various mechanical stresses. Studies have shown that the death and loss of NPC is an important cause of IVDD (Zhang et al., 2016).

Negative feedback regulation of the cellular death process is a key research direction to slow down IVDD. Ferroptosis is a form of regulated cell death distinguished by abnormalities in iron metabolism and an excessive build-up of lipid peroxides (Bogdan et al., 2016; Conrad et al., 2018; Ashrafizadeh, 2024). Iron overload and lipid peroxidation can result in reactive oxygen species (ROS) build-up. Under normal circumstances, the intracellular antioxidant system is activated to scavenge ROS; however, continuous production of ROS leads to a decrease of antioxidant enzyme activity or depletion of antioxidants and imbalance of the antioxidant system, which in turn triggers ferroptosis. Therefore, iron overload and antioxidant system imbalance are widely regarded as a primary mechanism leading to ferroptosis. At the same time, ferroptosis is connected to the IVDD process (Chen et al., 2022). Lu et al. (2021) directly measured the unstable iron pool in human NPC and found that the iron content was notably increased, and different concentrations of tert-butyl hydroperoxide (TBHP) were used to stimulate NPC. The iron level of NPC was significantly raised, and the cell morphology of ferroptosis was observed: mitochondria became smaller and mitochondrial membrane density agglutinated. Zhang et al. (2021) directly measured the iron level in IVDD and found that it was noticeably heightened, and the genes related to ferroptosis were significantly enriched. Yang et al. (2021b) stimulated mouse intervertebral disc tissue by TBHP to simulate the oxidative stress response of intervertebral disc and found that a high level of ferroptosis occurred in the treated intervertebral disc NPC. In summary, ferroptosis involves intervertebral disc NPC death, and ferroptosis inhibition can significantly alleviate the progression of IVDD.

MicroRNAs (miRNAs) inhibit the expression of genes mainly through the complementary 3' untranslated region of their target gene. Abundant evidence shows that miRNAs play a role in regulating various pathological processes (NPC apoptosis, inflammatory mediator infiltration, extracellular matrix metabolism) and is key for IVDD (Li et al., 2015; Cazzanelli and Wuertz-Kozak, 2020; Yang et al., 2021a). Up-regulation of miR-21 expression in IVDD tissues can lead to abnormal proliferation and cluster formation of NPC, causing the occurrence and development of IVDD (Liu et al., 2014). miR-377 is associated with extracellular matrix reorganization of intervertebral discs (Tsirimonaki et al., 2013). Other studies have shown that miR-4478 could worsen IVDD through intensifying oxidative stress in NPC (Zhang et al., 2023). In addition, ferroptosis is also regulated by miRNAs during IVDD. Over-expression of miR-874-3p can achieve negative regulation of transcription of activator 3, thereby inhibiting the ferroptosis process of NPC and delaying the progression of IVDD (Li et al., 2022). In summary, we can reasonably speculate that miR-4478 may promote the IVDD process by promoting the occurrence of ferroptosis.

Based on this hypothesis, this study used ferroptosis activator RSL3 to construct an *in vitro* NPC ferroptosis model (Yang et al., 2021b; Liu et al., 2023), detected the miR-4478 level and interfered with its expression to explore the effect of miR-4478 on NPC ferroptosis, and analysed its potential target genes. At the same time, the mouse IVDD model was used for *in vivo* verification, to provide novel insights into the IVDD occurrence and development, as well as new targets and new strategies for IVDD treatment.

Material and Methods

Cell grouping and processing

Human nucleus pulposus cells (NPC, CP-H097) were purchased from Punosai Life Technology Co., Ltd. (Wuhan, China). They were cultured in DMEM medium containing 10 % foetal bovine serum (C0235, Beyotime, Shanghai, China) and maintained at 37 °C in an environment with a volume fraction of 5 % CO_2.

SLC7A11 over-expression (SLC7A11) and negative control (vector), miR-4478 over-expression (mimics) and control (mimics NC), miR-4478 knockdown (inhibitor) and control (inhibitor NC) were purchased from RiboBio (Guangzhou, China). Subsequently, the cells were transfected with Lipofectamine 3000 (L3000001, Invitrogen, Waltham, MA), and all transfections were performed for 48 h.

NPC were implanted in 96-well plates at 5×10^6/l and treated with 0, 0.5, 1 μM RSL3 for 24 h to screen the optimal concentration of RSL3-induced cell damage. NPC were divided into control, ferroptosis model (RSL3), mimics, mimics NC, inhibitor, inhibitor NC and mimics+SLC7A11 groups. The cells in the control and RSL3 groups were cultured in DMEM for 48 h, and the other groups were transfected with miR-4478 and SLC7A11. After that, except for the control group, the other groups were treated with 1 μM RSL3 for 24 h to induce cell damage.

qRT-PCR

RNA was isolated from NPC by TRIzol™ (15596026CN, Invitrogen, Waltham, MA) and then reverse transcribed with AMV reverse transcriptase (2621, TAKARA, Tokyo, Japan) to obtain cDNA. The PCR reaction was done with TransStart Top Green qPCR SuperMix (AQ131-01, TRANS, Beijing, China). The reference genes were *U6* and *GAPDH*.

Primer sequences: *miR-4478*: F: 5'-CAGGGCTGCAGGGGATG-3'; R: 5'-CTGAGGAGCCTCCAAACCTG-3'; *SLC7A11*: F: 5'-TCCTGCTTTGGCTCCATGAACG-3'; R: 5'-AGAGGAGTGTGCTTGCGGACAT-3'; *U6*: F: 5'-CCCCTGGATCTTATCAGGCTC-3'; R: 5'-GCCATCTCCCCGGACAAAG-3'; *GAPDH*: F: 5'-GGAGCGAGATCCCTCCAAAAT-3'; R: 5'-GGCTGTTGTCATACTTCTCATGG-3'. The relative expression was calculated according to the $2^{-\Delta\Delta Ct}$ method.

CCK-8 assay

After the NPC were transfected and RSL3 was used to induce cell injury, 10 µl CCK-8 working solution (CA1210, Solarbio, Beijing, China) was added. The fully mixed cells were incubated at 37 °C for 2 h. The $OD_{450\ nm}$ value was determined with a microplate reader (1410101, Thermo Fisher Scientific, Waltham, MA) to calculate cell viability.

Calcein-AM/PI detection of live/dead cells

A Calcein-AM/PI kit (CA1630, Solarbio) was used to detect live/dead cells. NPC were grown in a 12-well plate, miR-4478 and SLC7A11 in NPC were over-expressed or knocked down, and then RSL3 was added to induce cell damage, digested with trypsin and collected for cell precipitation. The cells were washed with Assay Buffer and adjusted to 1×10^5 cells/ml, supplemented with 10 µl calcein-AM and incubated in the dark at 37 °C for 20 min. Thirty µl PI stock solution was added and staining was performed in the dark for 5 min. After that, the staining solution was discarded, the cells were resuspended after washing with PBS, and 3 µl of the cell solution was dropped on the slide. Then, a 490 nm excitation filter was used under a fluorescence microscope (MF52-N, Guangzhou Ming-Mei Technology Co., Ltd., Guangdong, China) to observe and capture the images. Calcein-AM displayed green fluorescence, while PI displayed red fluorescence, corresponding to the level of cell viability and death rate, respectively.

Determination of the ROS level in cells

A ROS detection kit (CA1410, Solarbio) was used to detect the ROS. NPC were collected, and the number of cells was adjusted to 1×10^6/ml. DCFH-DA was added at 1 : 1000 to an end concentration of 1 µmol/l, incubated at 37 °C for 30 min, washed with PBS and stimulated with a ROS-positive control for 30 min. The ROS level was detected by flow cytometry (FCM, BD FACSCaliburTM, BD Biosciences, Franklin Lakes, NJ).

Dual luciferase assay

The wild-type or mutant SLC7A11 3'UTR was inserted into the psicheck2.0 luciferase reporter vector to construct WT-SLC7A11 and MUT-SLC7A11 plasmids. WT-SLC7A11 and MUT-SLC7A11 were co-transfected with miR-4478 mimics or mimics NC into NPC using Lipofectamine 2000 (Invitrogen). After 48 h, luciferase activities were determined by a dual luciferase reporter gene assay kit (G06001, Gemma Gene, Shanghai, China).

Animal grouping and processing

Twenty-four SPF male C57BL/6J mice, 6 weeks old, weighing 20 ± 2 g, were provided by Spefor Biotechnology Co., Ltd. (Beijing, China). Mice were kept under normal conditions (temperature 20–24 °C, relative humidity 50–70 %, light and dark 12 h/12 h). This experiment was approved by the Zhongshan Hospital Affiliated to Fudan University Animal Ethics Committee.

Mice were randomly divided into a sham operation (Sham) group, model (IVDD) group, IVDD + miR-542-3p knockdown negative control (IVDD+antagomiR-NC) group and IVDD + miR-542-3p knockdown (IVDD+antagomiR-4478) group. The mice were anesthetized with intraperitoneal injection of 2 % pentobarbital sodium (50 mg/kg). In order to locate the position of the intervertebral disc, the muscle tissue was accurately stripped layer by layer from Co6 to Co8. A sterile 27G needle was inserted into the caudal vertebrae of mice (Co6/7 and Co7/8). The nucleus pulposus was used as the puncture object. The needle was rotated 360° and stayed in the intervertebral disc for 30 s. The needle was slowly pulled out and the puncture point was disinfected with an iodophor cotton ball. Finally, the wound was sutured layer by layer. After two weeks, 20 nM/kg antagomiR-NC or antagomiR-4478 solution was slowly injected into the punctured intervertebral disc with a 27-needle syringe (Sun et al., 2021; Jia et al., 2024). The Sham and IVDD groups were injected with the same amount of normal saline once every two weeks for 8 weeks, and then the mice were anesthetized and sacrificed by cervical dislocation, and the intervertebral disc tissue was stripped.

HE staining

The mouse intervertebral disc tissue was fixed with 4 % paraformaldehyde for 48 h and placed in the bone tissue decalcification solution (G1107, Servicebio, Wuhan, China) for decalcification for 2 days, dehydrated with ethanol gradient, embedded in paraffin, and the tissue specimens were cut into 5 µm thick sections. The sections were stained in haematoxylin solution for 5 min and with eosin (G1120, Solarbio) for 2 min. Then, the sections were sealed with neutral gum (G8590, Solarbio) and the intervertebral disc tissue structure was observed with a microscope (Axio, OLYMPUS, Tokyo, Japan).

Saffron solid green staining

After the paraffin sections of mouse intervertebral disc tissue were dewaxed to water, the sections were immersed in solid green staining (G1053, Servicebio) for 1 min. After rapid treatment with 1 % hydrochloric acid alcohol for 10 s, the sections were immersed in safranin staining solution for 3 min. After conventional dehydration and transparency treatment, the sections were sealed with neutral gum and the intervertebral disc structure was observed with a microscope.

Prussian blue staining

A Prussian blue staining kit (G1422, Solarbio) was used to detect ferritin and hemosiderin deposition in the intervertebral disc tissue. The paraffin sections of intervertebral disc tissue were stained by Perls working solution for 20 min, washed with distilled water and stained with nuclear fast red staining solution for 10 min. The sections were sealed with neutral gum and the tissue ferroptosis was detected with a microscope.

TUNEL staining

A TUNEL kit (C1086, Beyotime) was used to determine apoptosis in the intervertebral disc tissue. After the paraffin sections of intervertebral disc tissue were dewaxed to water, sections were permeabilized with proteinase K for 30 min, an appropriate amount of TUNEL working solution was added to stain for 60 min, and DAPI solution was added to stain the nucleus for 5 min. After sealing, the positive TUNEL staining was observed with a fluorescence microscope.

Fe^{2+} level determination

The Fe^{2+} levels in cells and tissues were measured using a ferrous ion content detection kit (BC5415, Solarbio). NPC were collected after different treatments and supernatants were collected following centrifugation at 1,000 *g* for 10 min at 4 °C. The intervertebral disc tissue and 5 times the volume of the extract were homogenized in an ice bath, and the supernatant was collected after centrifugation at 1,000 *g* for 10 min at 4 °C. Two hundred µl of supernatant, standard solution and reagent 1 were mixed in different centrifuge tubes and 100 µl of reagent 2 was added and incubated for 10 min. Then, 100 µl of chloroform was added for vortex mixing for 5 min. After centrifugation, 200 µl of the upper solution was extracted and placed in 96-well plates. The $OD_{593\ nm}$ value was measured by a microplate reader and the Fe^{2+} content was calculated.

Determination of antioxidant enzyme levels

NPC were collected after different treatments. The intervertebral disc tissues of mice were homogenized and the supernatants were collected after centrifugation at 1,200 *g* for 10 min at 4 °C. A malondialdehyde (MDA) kit and glutathione (GSH) kit (A003-4-1, A006-2-1, Nanjing Jiancheng Bioengineering Institute, Nanjing, China) were used to determine the level of antioxidant enzymes. The contents of MDA and GSH in NPC were determined following the suppliers' instructions. The $OD_{450\ nm}$ value was measured by a microplate reader and the enzyme content of each group was calculated.

Western blot (WB)

After different treatments, NPC and intervertebral disc tissue were collected and the supernatant was fully lysed. The protein concentration after lysis was determined. The same amount of protein was used for SDS-PAGE electrophoresis and then transferred to PVDF membrane (YA1700, Solarbio). After washing with TBST buffer, the cells were incubated with 5 % skimmed milk powder (LP0033B, Solarbio) at room temperature for 2 h. Nuclear factor E2-related factor 2 (Nrf2, ab313825, 1 : 1000), glutathione peroxidase 4 (GPX4, ab125066, 1 : 1000), ferritin heavy chain 1 (FTH1, ab183781, 1 : 1000), acyl-CoA synthetase long-chain family member 4 (ACSL4, ab155282, 1 : 10,000), cyclooxygenase 2 (COX-2, ab179800, 1 : 2000), solute carrier family 7 member 11 (SLC7A11, ab307601, 1 : 1000) and GAPDH (ab8245, 1 : 1000) antibodies were added and incubated overnight at 4 °C. On the next day, the TBST buffer (T1082, Solarbio) was washed and secondary antibody (1 : 20,000) was added and incubated for 1 h. The ECL reagent (PE0010, Solarbio) was used to develop colour for 2 min, and then the chemiluminescence imaging system (Tanon 5200 Multi, Tianneng Technology Co., Ltd., Shanghai, China) was used for imaging. The grey scale of the strips was analysed with Image J software.

Statistical analysis

The experiments were repeated three times independently and the measurement data of normal distribution were expressed as mean ± standard deviation. Statistical analysis was performed by Prism software (Graph pad 9.0). Student's *t*-test was used to analyse the differences between two groups and one-way ANOVA analysis was used to compare multiple groups. $P < 0.05$ was regarded as statistically significant.

Results

miR-4478 is highly expressed in ferroptosis of NPC

RSL3 is one of the earliest identified ferroptosis inducers. Targeted inhibition of GPX4 could produce ROS and trigger ferroptosis without GSH consumption (Dixon et al., 2012). Nrf2 can target a series of redox-related genes and is key for reducing ferroptosis (Dodson et al., 2019). GPX4 is a negative regulator and specific marker of ferroptosis (Liu et al., 2021). Therefore, in order to clarify the optimal induction concentration of RSL3, we detected Nrf2 and GPX4 protein expression after ferroptosis induced by 0, 0.5, 1 µM RSL3, so as to judge whether the NPC ferroptosis model was successfully constructed. Nrf2 and GPX4 levels declined remarkably with RSL3 concentration increase (Fig. 1A–C), indicating that NPC ferroptosis induced by 1 µM RSL was the most obvious, so the NPC ferroptosis model was effectively constructed. Simultaneously, the *miR-4478* level was detected, and it increased markedly with the RSL3 concentration raise. When the RSL concentration was 1 µM, *miR-4478* was the highest (Fig. 1D). Ultimately, the induction effect of 1 µM RSL was the best, ferroptosis was the most obvious and miR-4478 was the highest. Therefore, 1 µM RSL was used to treat the mouse intervertebral disc NPC to induce ferroptosis in subsequent experiments.

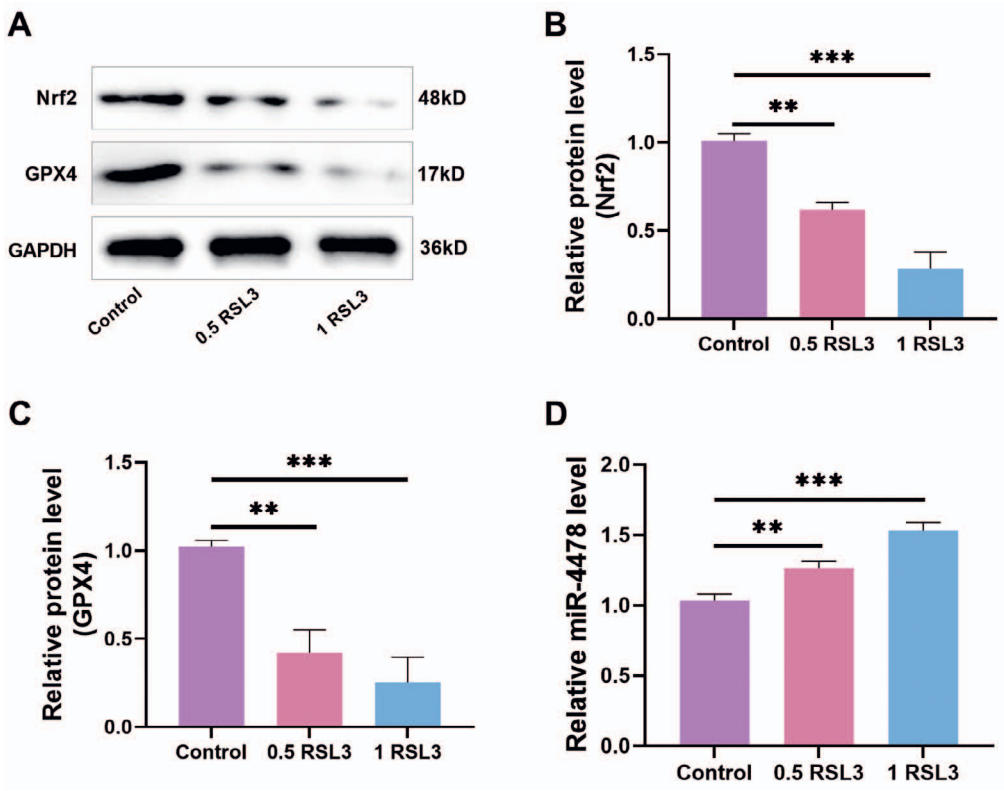

Fig. 1. miR-4478 is highly expressed in ferroptosis of NPC. (**A**–**C**) Nrf2 and GPX4 protein expression after ferroptosis induced by different concentrations of RSL3 was discerned by WB. It can be seen that their expression was the lowest after 1 μM RSL3 induction. (**D**) The *miR-4478* level after ferroptosis induced by different concentrations of RSL3 was discerned by qRT-PCR, and it was found that it was the highest after 1 μM RSL3 induction.
N = 3, $^{**}P < 0.01$, $^{***}P < 0.001$.

Over-expression and knockdown of miR-4478 can affect ferroptosis in NPC

To elucidate the specific connection between miR-4478 and ferroptosis in NPC, we used 1 μM RSL3 to induce ferroptosis in NPC, and over-expressed or knocked down miR-4478. First, the transfection efficiency was tested. The miR-4478 level was significantly increased or decreased (Fig. 2A–B), suggesting that subsequent experiments could be performed. The cell viability was significantly decreased after ferroptosis of NPC and it was further reduced after over-expression of miR-4478, but the cell viability was significantly increased after knockdown of miR-4478 (Fig. 2C), indicating that knockdown of miR-4478 had an improving effect on RSL3-induced cell injury. Next, we detected the live and dead cells by calcein-AM/PI staining. After NPC ferroptosis, calcein-AM-labelled live cells were significantly reduced and PI-labelled dead cells were significantly increased. After over-expression of miR-4478, the cell damage was further aggravated, but it was significantly reversed after its knockdown (Fig. 2F–H). In conclusion, knockdown of miR-4478 attenuates RSL3-induced cell injury by increasing NPC survival and reducing cell death, while over-expression of miR-4478 aggravates RSL3-induced cell injury.

Ferroptosis is characterized by iron metabolism disorders and antioxidant system inactivation, causing accumulation of lipid peroxides and ROS (Conrad et al., 2018; Han et al., 2020), resulting in fatal damage to cells. The MDA content can indicate the extent of lipid peroxidation in the body and indirectly represent the level of cellular damage. GSH can scavenge free radicals and protect intracellular biomolecules from oxidative damage. We detected MDA and GSH contents in NPC treated with different treatments using appropriate kits. The results showed that after NPC ferroptosis, MDA increased significantly and GSH lessened significantly. This phenomenon was further aggravated after over-expression of miR-4478, but MDA and GSH were notably reduced and enhanced after knockdown of miR-4478 (Fig. 2E and I). Then, the ROS intensity in NPC was discovered, and the results were consistent with the MDA content change trend, that is, the ROS intensity was significantly increased after RSL3 induction, but the intensity was significantly decreased after miR-4478 knockdown (Fig. 2J–K). Overall, knockdown of miR-4478 can increase the activity of antioxidant enzymes, reduce ROS accumulation and reduce the oxidation reaction in NPC.

Fe^{2+} interacts with hydrogen peroxide to generate hydroxyl radicals, which then react with polyunsaturated

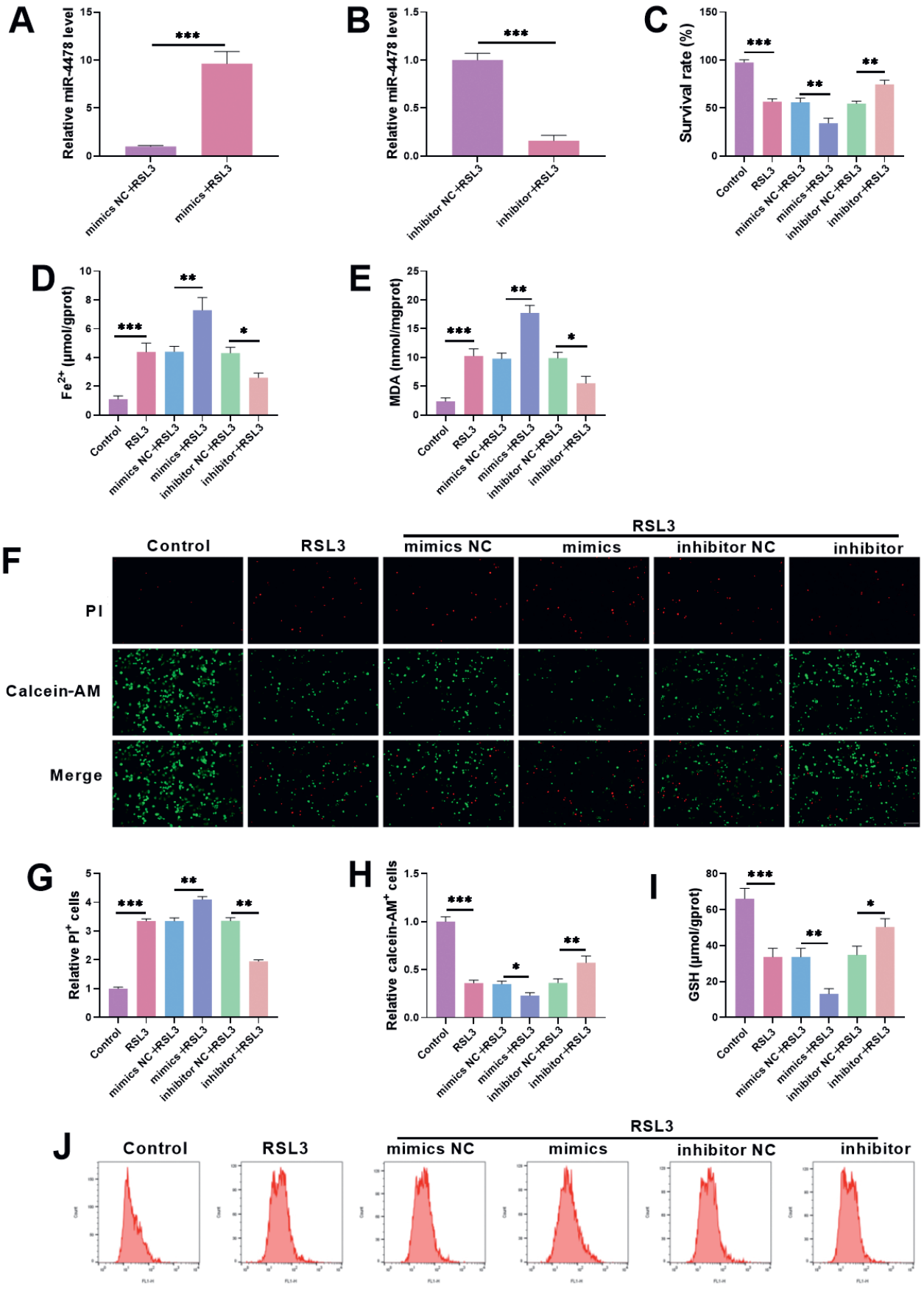
A
Relative miR-4478 level
mimics NC+RSL3
mimics+RSL3
B
Relative miR-4478 level
inhibitor NC+RSL3
inhibitor+RSL3
C
Survival rate (%)
Control
RSL3
mimics NC+RSL3
mimics+RSL3
inhibitor NC+RSL3
inhibitor+RSL3
D
Fe2+ (μmol/gprot)
E
MDA (nmol/mgprot)
F
RSL3
Control
RSL3
mimics NC
mimics
inhibitor NC
inhibitor
PI
Calcein-AM
Merge
G
Relative PI+ cells
H
Relative calcein-AM+ cells
I
GSH (μmol/gprot)
J
RSL3
Control
RSL3
mimics NC
mimics
inhibitor NC
inhibitor

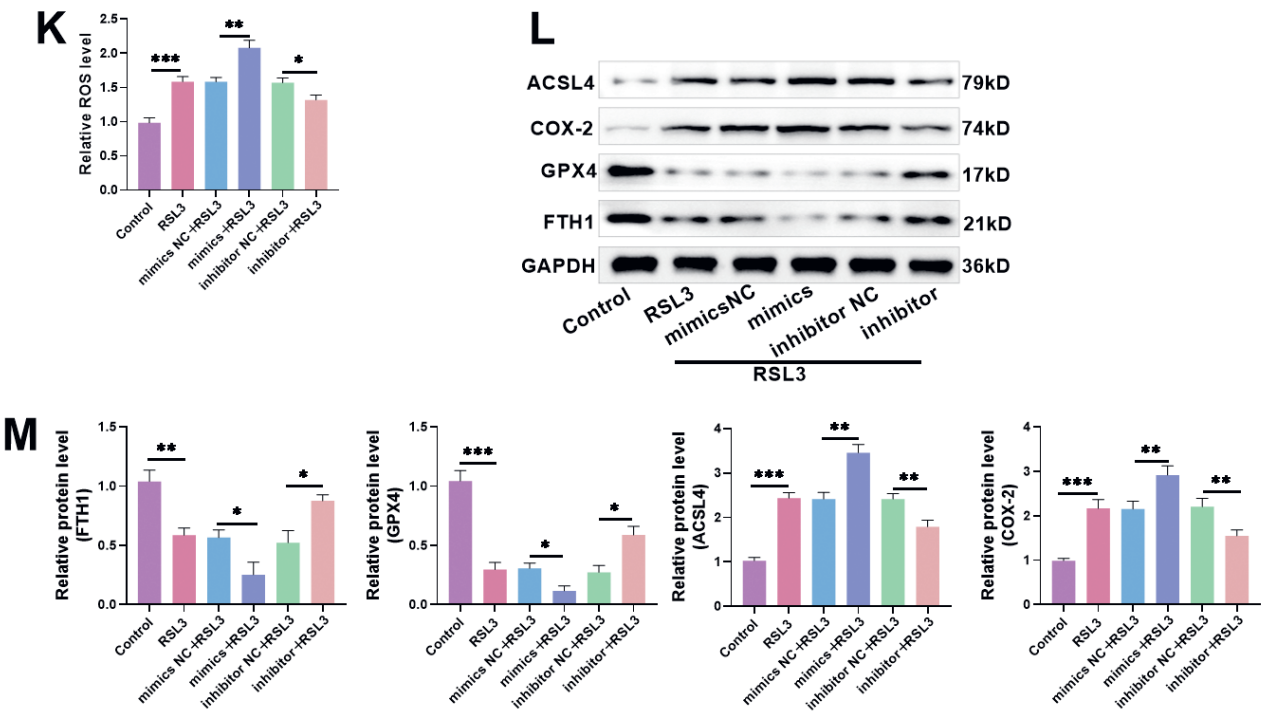

Fig. 2. Over-expression and knockdown of miR-4478 can affect ferroptosis in NPC. (**A**–**B**) qRT-PCR showed that *miR-4478* was effectively over-expressed or knocked down. (**C**) The survival rate of NPC under different treatment conditions was tested with CCK-8. It was found that the survival rate of NPC was significantly decreased after RSL3 induction. The cell survival rate was further decreased after over-expression of miR-4478, but the cell survival rate was notably increased after silencing miR-4478. (**D**) The Fe^{2+} level raised notably after RSL3 induction, further increased after miR-4478 over-expression, and significantly decreased after miR-4478 knockdown. (**E**, **I**) The MDA content increased significantly and GSH content decreased significantly after ferroptosis of NPC. The phenomenon was further aggravated after over-expression of miR-4478, and the effect was significantly weakened after knockdown of miR-4478. (**F**–**H**) Calcein-AM/PI was used to detect the live and dead cells. It was found that the live cells diminished noticeably and the dead cells increased markedly after NPC ferroptosis. After miR-4478 over-expression, the live cells decreased further and the dead cells increased further. After miR-4478 knockdown, the live cells increased significantly and the dead cells decreased significantly (×20, 100 μm). (**J**–**K**) The ROS level in the cells was tested by FCM. It increased noticeably after RSL3 induction. The level of ROS increased further after miR-4478 over-expression and decreased significantly after miR-4478 knockdown. (**L**–**M**) WB detection of ferroptosis-related proteins showed that FTH1 and GPX4 were notably decreased after RSL3 induction, while ACSL4 and COX-2 were increased. The ferroptosis effect was more serious after miR-4478 over-expression and it was effectively alleviated after miR-4478 knockdown.
N = 3, $^{*}P < 0.05$, $^{**}P < 0.01$, $^{***}P < 0.001$.

fatty acids to produce lipid peroxides, subsequently initiating ferroptosis (Galaris et al., 2019). Therefore, we detected the level of Fe^{2+} in NPC, and the Fe^{2+} level raised remarkably after RSL3 induction. The level of Fe^{2+} increased further after over-expression of miR-4478 but decreased significantly after its knockdown (Fig. 2D). In addition, FTH1 is an iron storage protein, it has the ferric oxygenase function and diminishes Fe^{2+} toxicity (Salatino et al., 2019). ACSL4 and COX-2 are key for the regulation of ferroptosis (Yuan et al., 2016; Hashemi Goradel et al., 2019). Therefore, we detected ferroptosis-related protein expression. The effects of RSL3 and miR-4478 on the protein expression in NPC were consistent with the previous results. After RSL3 induction, FTH1 and GPX4 diminished noticeably, while ACSL4 and COX-2 increased substantially. Ferroptosis was further aggravated after over-expression of miR-4478, but it was alleviated after knockdown (Fig. 2L–M). Finally, miR-4478 has a regulatory effect on iron metabolism in cell injury. In conclusion, knockdown of miR-4478 can alleviate ferroptosis in NPC by stabilizing iron metabolism and reducing the oxidation level, while over-expression of miR-4478 can aggravate ferroptosis in NPC.

miR-4478 can target down-regulate the expression of SLC7A11

The potential target gene of miR-4478 was identified as *SLC7A11* by miRWalk and TargetScan databases; therefore, we investigated the SLC7A11 level. The SLC7A11 level was notably declined after RSL3 treat-

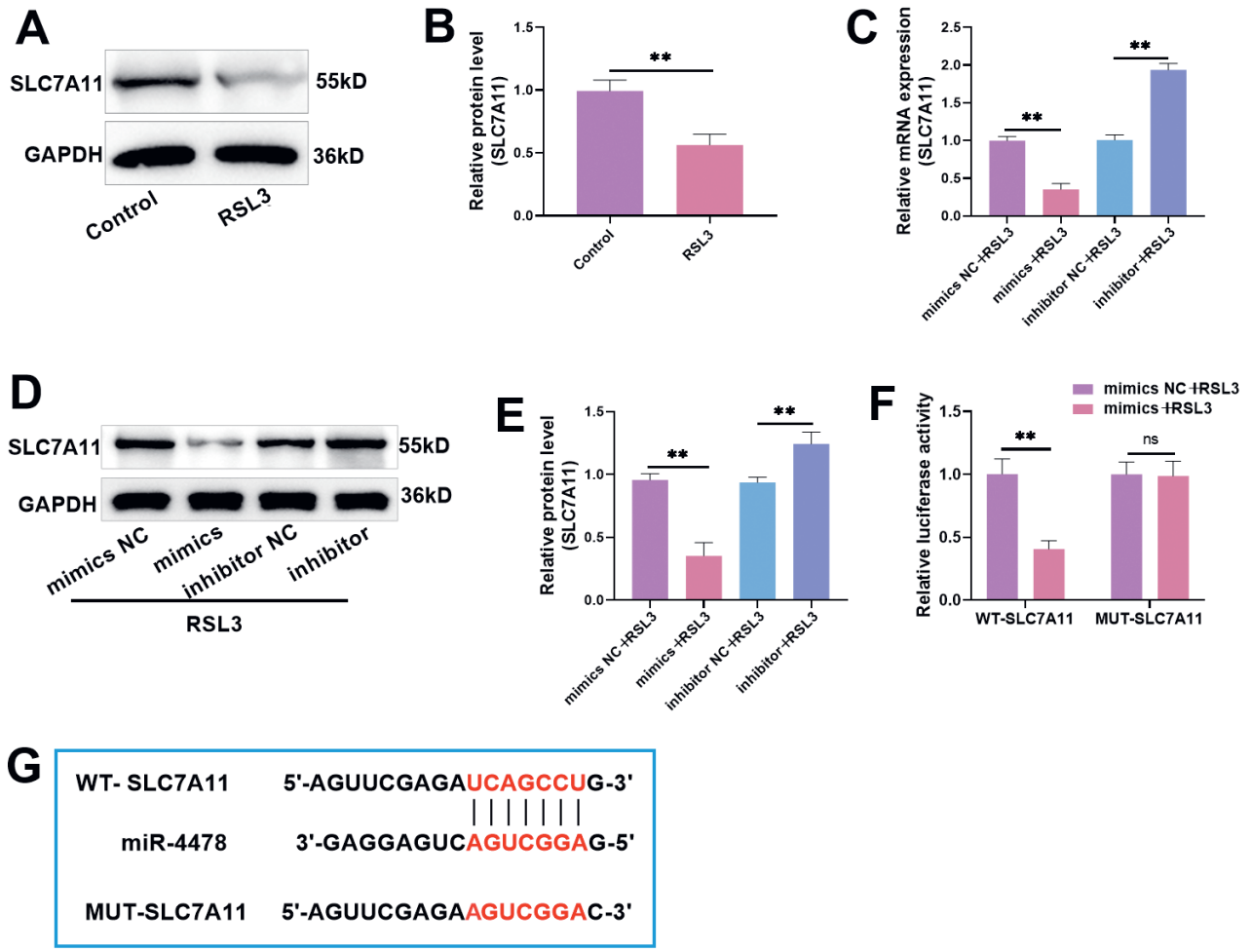

Fig. 3. miR-4478 can target down-regulate the expression of SLC7A11. (**A**–**B**) The WB-detected protein level of SLC7A11 after RSL3 induction was significantly reduced. (**C**–**E**) qRT-PCR- and WB-detected *SLC7A11* gene and SLC7A11 protein levels after miR-4478 over-expression or knockdown were significantly reduced or increased, respectively. (**F**) The luciferase reporter plasmids of WT-SLC7A11 and MUT-SLC7A11 were co-transfected into NPC with mimics NC and mimics, respectively, and luciferase activity was detected. The heightened level of miR-4478 noticeably inhibited WT-SLC7A11 luciferase activity. (**G**) The binding sequence of miR-4478 and *SLC7A11*.
N = 3, $^{**}P < 0.01$.

ment (Fig. 3A–B), suggesting a potential protective effect of SLC7A11 in RSL3-induced ferroptosis of NPC. The SLC7A11 level was markedly decreased after over-expression of miR-4478 and significantly increased after knockdown of miR-4478 (Fig. 3C–E), indicating that miR-4478 can target *SLC7A11*. Next, we used a luciferase reporter to check whether miR-4478 and SLC7A11 bind each other. miR-4478 over-expression could noticeably inhibit WT-SLC7A11 luciferase activity but had no notable influence on MUT-SLC7A11 (Fig. 3F), indicating that miR-4478 could bind to *SLC7A11*. There is a potential binding site between miR-4478 and *SLC7A11*, and the binding sequence is shown in Fig. 3G. In conclusion, miR-4478 can target down-regulate the expression of *SLC7A11*.

miR-4478 promotes ferroptosis of NPC by inhibiting SLC7A11

Informed by the above findings, we further investigated whether miR-4478 could target the SLC7A11 level to affect ferroptosis in NPC. We first verified the over-expression efficiency of SLC7A11 and found that the SLC7A11 protein was successfully over-expressed (Fig. 4A–B), indicating that further experiments could be conducted. The NPC were split into a model (mimics NC+Vector) group, miR-4478 over-expression (mimics+Vector) group and miR-4478 over-expression + SLC7A11 over-expression (mimics+SLC7A11) group. Similar to the previous results, miR-4478 over-expression aggravated RSL3-induced NPC cell damage, iron metabolism disorder and oxidation level. On this basis, SLC7A11 was over-expressed, and the survival rate of

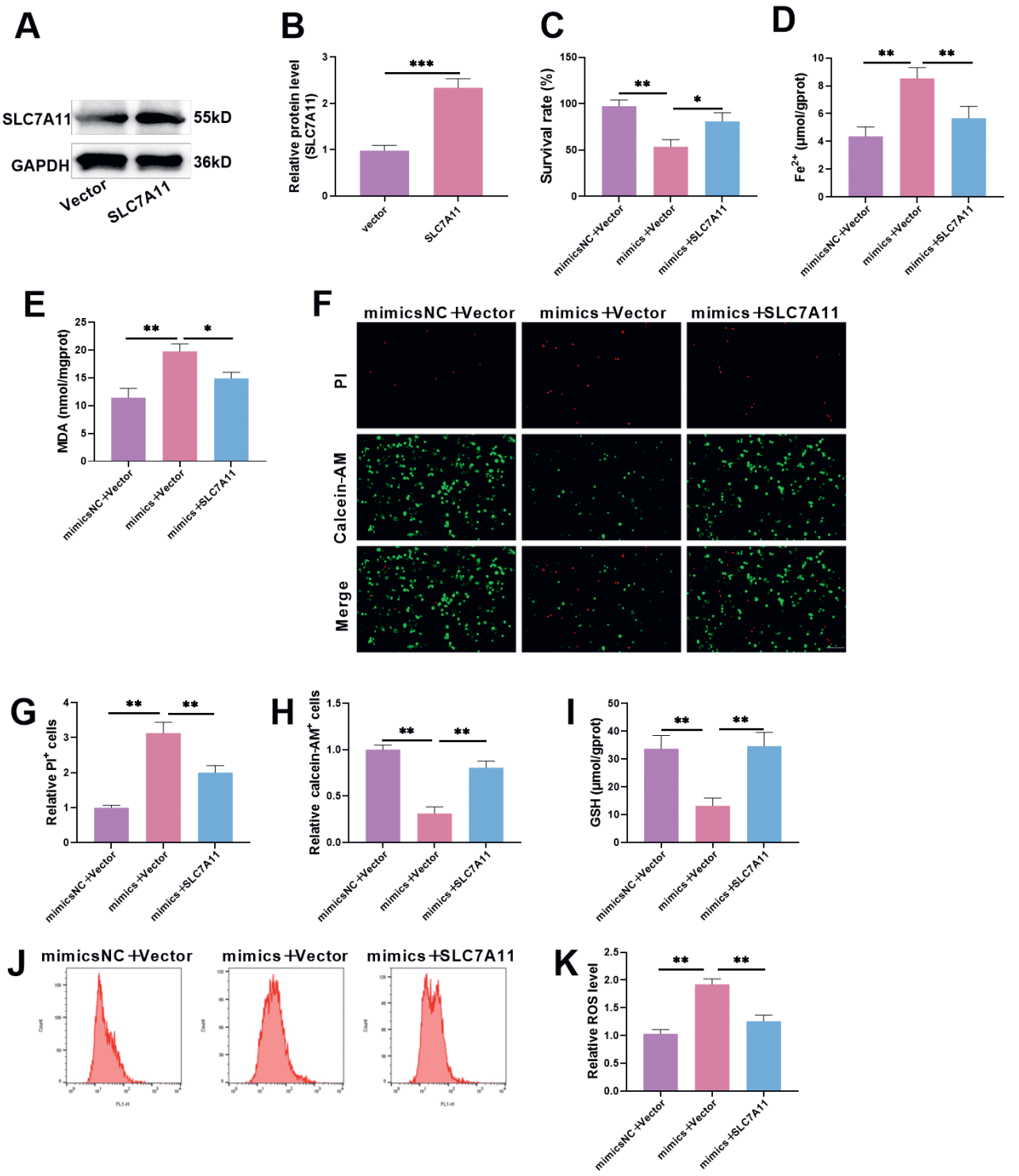

Fig. 4. miR-4478 promotes ferroptosis of NPC by inhibiting SLC7A11. (**A**–**B**) WB detection of SLC7A11 over-expression efficiency showed that the SLC7A11 protein was effectively highly expressed. (**C**) The survival rate of NPC was tested with CCK-8 and was significantly increased after SLC7A11 over-expression compared with miR-4478 over-expression alone. (**D**) After over-expression of SLC7A11, the level of Fe^{2+} was significantly lower than that of miR-4478 alone. (**E**, **I**) Compared with miR-4478 over-expression alone, the MDA content was noticeably reduced and the GSH content was significantly raised after SLC7A11 over-expression. (**F**–**H**) Calcein-AM/PI detection of live and dead cells. Compared with miR-4478 over-expression alone, SLC7A11 over-expression showed a considerable increase in live cells and a substantial reduction in dead cells (×20, 100 μm). (**J**–**K**) The ROS level in cells was tested by FCM. After over-expression of SLC7A11, it was significantly lower than that of miR-4478 alone.
N = 3, $^{*}P < 0.05$, $^{**}P < 0.01$, $^{***}P < 0.001$.

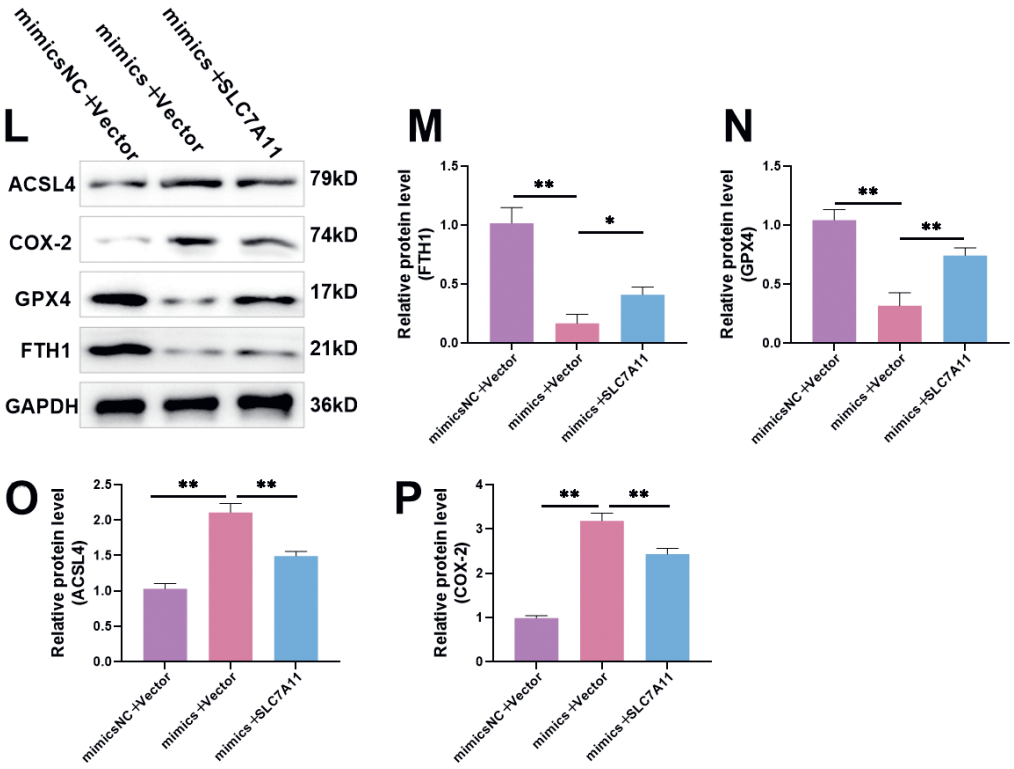

Fig. 4. miR-4478 promotes ferroptosis of NPC by inhibiting SLC7A11. (**L**–**P**) WB was used to detect ferroptosis-related proteins. Compared with miR-4478 over-expression alone, FTH1 and GPX4 were markedly increased after SLC7A11 over-expression, while ACSL4 and COX-2 were notably diminished.
N = 3, $^{*}P < 0.05$, $^{**}P < 0.01$, $^{***}P < 0.001$.

NPC was significantly increased (Fig. 4C). Calcein-AM-labelled live cells were significantly increased, and PI-labelled dead cells were significantly reduced (Fig. 4F–H). The Fe^{2+} level (Fig. 4D), MDA content (Fig. 4E) and ROS intensity (Fig. 4J–K) were markedly lessened, and the GSH content was considerably elevated (Fig. 4I). The expression trends of GPX4, FTH1, COX-2 and ACSL4 aligned with the previous findings (Fig. 4L–P). This indicated that SLC7A11 over-expression significantly attenuated the facilitating influence of miR-4478 over-expression on RSL3-induced ferroptosis. Combined with bioinformatic results, it was shown that miR-4478 can target down-regulate SLC7A11 to promote ferroptosis of NPC, and its mechanism is related to aggravation of iron metabolism disorder and oxidation level.

Knockdown of miR-4478 can improve tissue damage in mice with IVDD

In view of the function of miR-4478 *in vitro*, we further explored the contribution of miR-4478 in IVDD mice. AntagomiR-NC and antagomiR-4478 were injected into the caudal vertebra. The experimental procedure is shown in Fig. 5A, and then related tests were performed. HE and saffron solid green staining showed that the Sham group had a clear structural framework, clear boundaries between annulus fibrosus and nucleus pulposus, and highly saturated intervertebral space. In IVDD and IVDD+antagomiR-NC groups, the nucleus pulposus tissue was lost, the border between it and annulus fibrosus was blurred, and the intervertebral height was significantly reduced. Knockdown of miR-4478 softened the nucleus pulposus tissue loss and intervertebral disc structure destruction (Fig. 5B–C). The apoptosis was expanded notably in IVDD mice and decreased significantly after miR-4478 knockdown (Fig. 5D–E). In conclusion, knockdown of miR-4478 can improve IVDD by maintaining the intervertebral disc tissue structure and reducing apoptosis.

Knockdown of miR-4478 reduced ferroptosis in IVDD mice

Previous results have shown that miR-4478 can regulate ferroptosis *in vitro*, so we further verified whether miR-4478 can regulate ferroptosis in IVDD mice. Prussian blue staining showed that the blue particles in IVDD and IVDD+antagomiR-NC groups were markedly abundant, indicating that the iron deposition was seriously elevated. After miR-4478 knockdown, the number of the blue particles decreased and the proportion of Prussian blue-positive discs decreased (Fig. 6A), indicating that miR-4478 knockdown inhibited intervertebral disc iron deposition. In addition, we also found

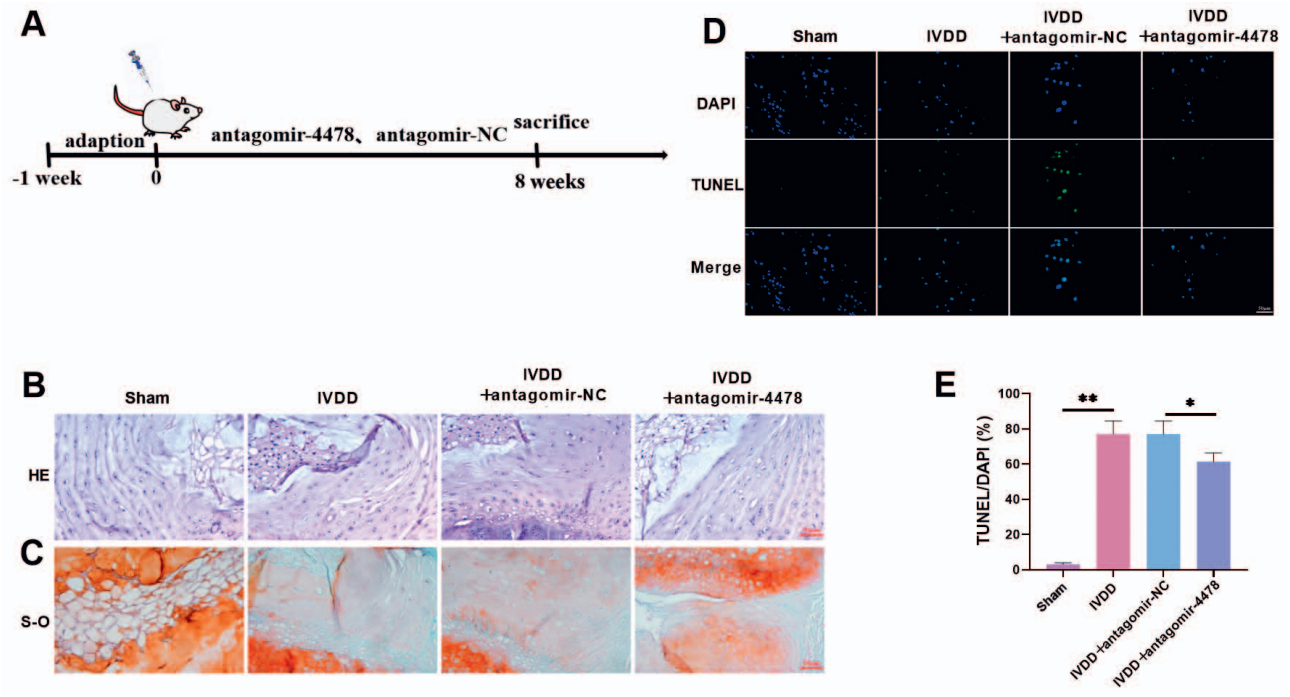

Fig. 5. Knockdown of miR-4478 can improve tissue damage in mice with IVDD. (**A**) Experimental flow chart. (**B**–**C**) HE and saffron solid green staining results showed that the nucleus pulposus tissue of IVDD mice was lost, the border between the annulus fibrosus and the nucleus pulposus was blurred, and the intervertebral height was significantly reduced; the intervertebral disc structure was restored after miR-4478 knockdown (×40, 50 μm). (**D**–**E**) TUNEL detection showed a substantial rise in apoptosis in IVDD mice, which was significantly reduced after miR-4478 knockdown (×40, 50 μm). N = 3, $^{*}P < 0.05$, $^{**}P < 0.01$.

that the expression trends of oxidation indicators, Fe^{2+}, SLC7A11 and ferroptosis-related proteins in intervertebral disc tissues after miR-4478 knockdown were consistent with the previous results (Fig. 6B–J), indicating that knockdown of miR-4478 can reduce ferroptosis by improving iron metabolism and oxidation levels. In conclusion, knockdown of miR-4478 can improve IVDD by reducing ferroptosis and maintaining the intervertebral disc tissue structure.

Discussion

At present, clinical treatment can only alleviate lumbago symptoms of IVDD and cannot fundamentally prevent further degeneration. Therefore, it is of great clinical value to actively develop drugs that can effectively delay IVDD for a long time (Krut et al., 2021). In this study, the NPC ferroptosis cell model was established by RSL3 induction and the IVDD mouse model was established by acupuncture. RSL3 could elicit significant reduction of NPC ferroptosis markers Nrf2 and GPX4. At the same time, the annulus fibrosus structure of IVDD mice was damaged, the nucleus pulposus tissue was lost, and the nucleus pulposus cells were shrunk and deformed, their number was reduced, showing that the model was effectively established.

The study also showed that the miR-4478 level was notably enhanced in NPC ferroptosis, suggesting that the miR-4478 increase may promote the occurrence of IVDD. Studies have reported that miR-4478 accelerates oxidative stress in NPC to aggravate IVDD (Zhang et al., 2023), and ferroptosis is often secondary to disorders of the antioxidant system. The pathological process of IVDD mainly includes intervertebral disc tissue injury, cartilage matrix loss and NPC apoptosis, among which the death of NPC is the main cause (Zhang et al., 2016). Therefore, inhibition of ferroptosis can significantly alleviate the progression of IVDD (Lu et al., 2021; Lu and Zheng, 2023). Therefore, we speculate that miR-4478 can promote ferroptosis of NPC and significantly promote the progression of IVDD. In order to prove this speculation, this study analysed the miR-4478 effect on ferroptosis by interfering with its expression. The elevated miR-4478 level could reduce the survival of NPC and increase their death. Further studies found that miR-4478 could significantly increase ROS, MDA and Fe^{2+} content, excessive consumption of antioxidants such as GSH and GPX4, and significantly reduce the FTH1 protein level, increase COX-2 and ACSL4 protein levels, but the above indicators were reversed after miR-4478 was knocked down. It has been reported that ferroptosis is driven by accumulation of Fe ions and production of ROS, which produces many lipid perox-

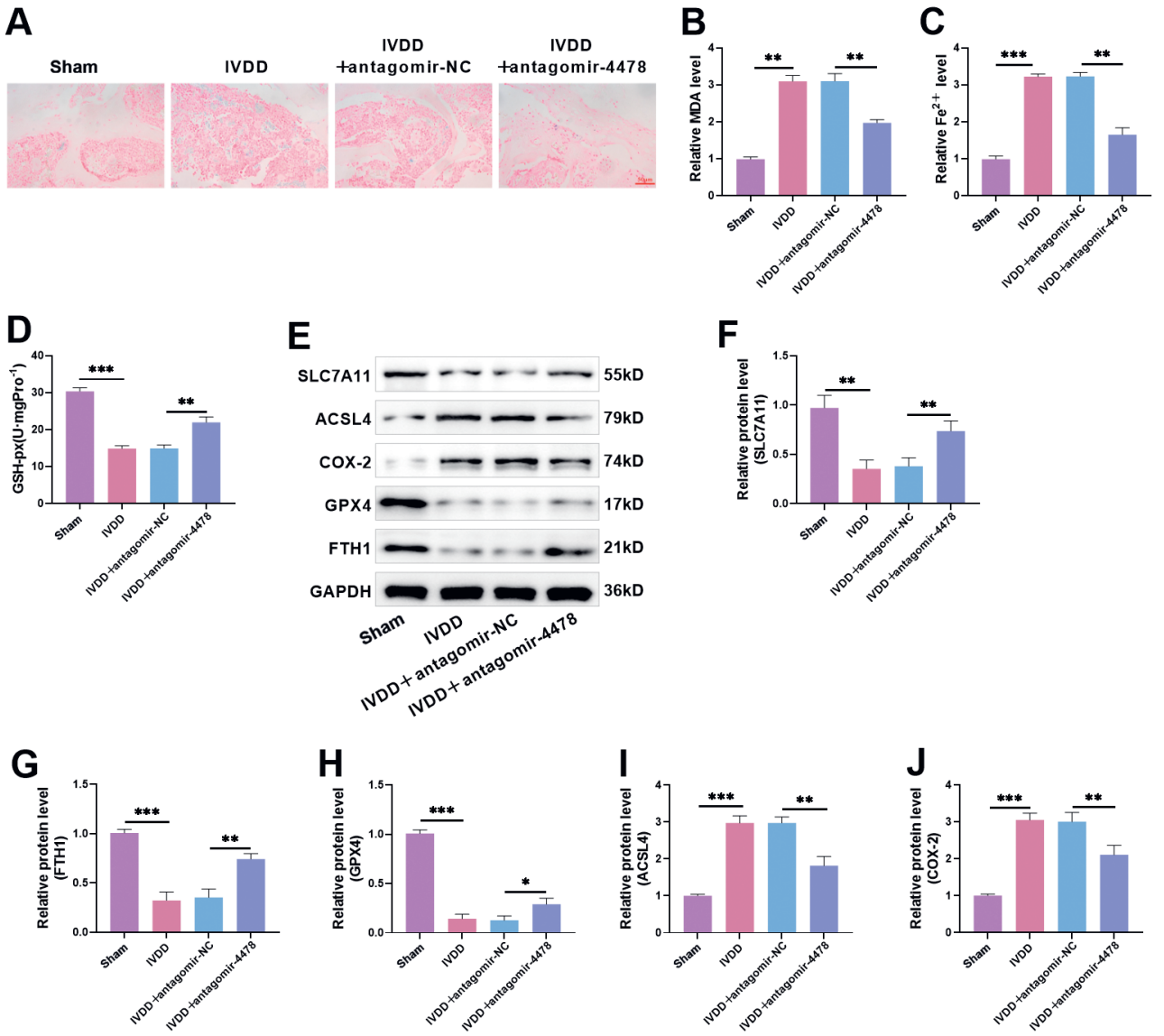

Fig. 6. Knockdown of miR-4478 reduced ferroptosis in IVDD mice. (**A**) Prussian blue staining showed that IVDD mice had severe intervertebral disc iron deposition, which was effectively alleviated after miR-4478 knockdown (×40, 50 μm). (**B**, **D**) The MDA content was markedly heightened and the GSH content was notably decreased in IVDD mice, which was significantly reversed after miR-4478 knockdown. (**C**) The level of Fe^{2+} in NPC of IVDD mice was raised remarkably and decreased after miR-4478 knockdown. (**E**–**J**) WB detection of SLC7A11 and ferroptosis-related proteins showed that the levels of SLC7A11, FTH1 and GPX4 in IVDD mice were dramatically lowered, ACSL4 and COX-2 were considerably increased and miR-4478 was significantly reduced after knockdown.
N = 3, $^{**}P < 0.01$, $^{***}P < 0.001$.

ides (Jiang et al., 2021). Oxidative stress is viewed as the principal cause of ferroptosis (Yu et al., 2021). MDA and GSH are key regulatory enzymes in lipid peroxidation of ferroptosis, which can lead to increased intracellular ROS accumulation, further aggravating cell damage (Jin et al., 2023) and abnormal expression of ferroptosis-related proteins (Nishizawa et al., 2020; Fratta Pasini et al., 2023). GPX4 is the key regulatory factor causing ferroptosis; the inactivation of GPX4 results in production of peroxides in NPC, leading to ferroptosis (Chen et al., 2021; Wu et al., 2021). FTH1 regulates intracellular iron concentration by storing free iron ions and reduces iron toxicity caused by free radical production (Cui et al., 2023). ACSL4 is a crucial factor in determining sensitivity to ferroptosis (Doll et al., 2017). COX-2 participates in the inflammatory cascade and is also a peroxidase involved in ferroptosis (Hashemi Goradel et al., 2019). It is suggested that miR-4478 over-expression could enhance ferroptosis in NPC via increasing oxidative stress and iron metabolism disorders, indicating that it could be a possible target for IVDD targeted treatment.

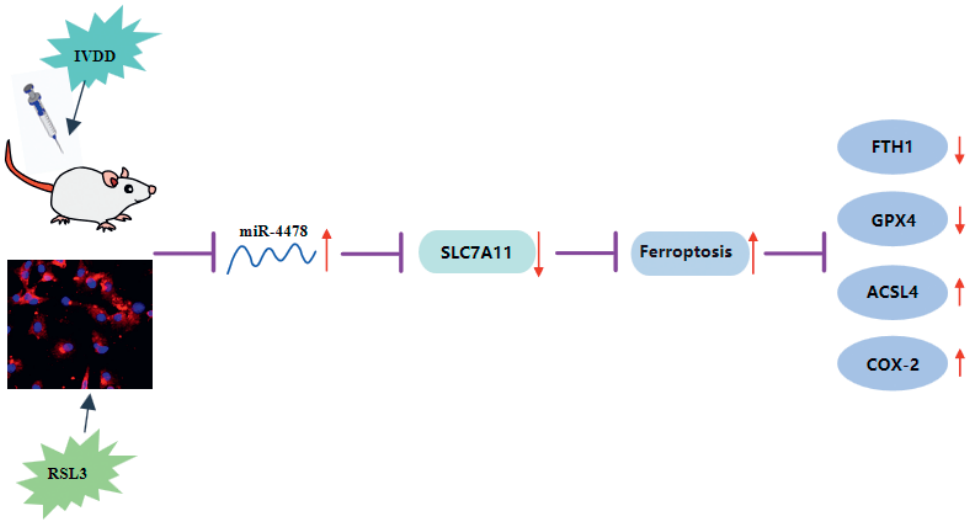

Fig. 7. The mechanism of miR-4478 promoting ferroptosis in NPC. miR-4478 is highly expressed in intervertebral disc degeneration, which can promote nucleus pulposus cell ferroptosis through targeting SLC7A11 to cause iron metabolism dysregulation and peroxide accumulation in nucleus pulposus cells.

In addition, the SLC7A11 level was notably decreased in RSL3-induced NPC ferroptosis, and the potential target of miR-4478 was *SLC7A11* using bioinformatic assessment, with detected potential binding sites, indicating that miR-4478 could target *SLC7A11*. SLC7A11 can promote biosynthesis of GSH, increase GPX4 activity, prevent build-up of lipid peroxidation products and prevent ferroptosis (Koppula et al., 2018). Studies have shown that SLC7A11 is the main regulatory transporter that mediates the GSH synthesis pathway. Inhibition of SLC7A11 expression can reduce GSH synthesis, reduce GPX4 activity and promote ferroptosis (Zeng et al., 2022). However, it is uncertain whether miR-4478 can diminish ferroptosis of NPC by targeting SLC7A11. Therefore, we simultaneously over-expressed SLC7A11 and miR-4478. The survival rate of NPC raised markedly, the mortality rate decreased significantly, ROS, MDA and Fe^{2+} levels decreased notably, GSH, GPX4 and FTH1 levels increased remarkably, and COX-2 and ACSL4 proteins decreased visibly, indicating that SLC7A11 over-expression could reduce the degree of ferroptosis of NPC and weaken the promoting effect of miR-4478p over-expression. Combined with bioinformatic results, miR-4478 can promote ferroptosis of NPC by inhibiting SLC7A11.

Finally, we verified the function of miR-4478 in IVDD *in vivo*. The IVDD mouse model was established by the acupuncture method. It was found that the structure of intervertebral disc tissue was damaged and the nucleus pulposus tissue was lost. Prussian blue staining showed that iron deposition increased, GSH content decreased, SLC7A11, GPX4 and FTH1 levels decreased significantly, and MDA, Fe^{2+}, COX-2 and ACSL4 levels increased significantly. This may be due to the damage of electron transport chain function after mitochondrial damage, contributing to a higher Fe^{2+} level and excessive consumption of antioxidants such as GPX4 (Fu et al., 2022; Huang et al., 2023). The discs showed ferroptosis; when miR-4478 was knocked down, the intervertebral disc structure destruction was reduced, iron deposition was reduced, GSH, SLC7A11, GPX4 and FTH1 levels were significantly increased, MDA, Fe^{2+}, COX-2 and ACSL4 levels were significantly reduced, and apoptosis was significantly reduced, indicating that knockdown of miR-4478 could reduce ferroptosis by improving iron metabolism and oxidation levels, thereby improving IVDD.

Conclusion

Overall, this analysis revealed the mechanism of miR-4478 effects on NPC ferroptosis in IVDD. Overexpression of miR-4478 can promote oxidative stress and iron metabolism disorders by inhibiting SLC7A11 and promote NPC ferroptosis to induce IVDD, indicating that miR-4478 is expected to become a biomarker target for IVDD therapy, which holds considerable importance for the diagnosis, treatment and outcome of IVDD. However, there are some limitations in this study. The regulatory system of miR-4478 has not been studied in depth in the ferroptosis process, and the related signalling pathways of miR-4478 regulating ferroptosis have not been analysed, which needs to be further explored.

Consent to publish

The manuscript has neither been previously published nor is under consideration by any other journal. The authors have all approved the content of the paper.

Ethic approval

This experiment was approved by the Zhongshan Hospital Affiliated to Fudan University Animal Ethics Committee.

Data availability statement

The data that support the findings of this study are available from the corresponding author upon request.

Author contribution

[Dongliang Gong, Long Jia]: Developed and planned the study, performed experiments and interpreted results. Edited and refined the manuscript with a focus on critical intellectual contributions.

[Yuhang Wang, Chengwei Xu, Xuxing Sun]: Participated in collecting, assessing and interpreting the data. Made significant contributions to data interpretation and manuscript preparation.

[Xiao Wu, Xiaojun Han]: Provided substantial intellectual input during the drafting and revision of the manuscript.

Conflicts of interest

The authors declare that they have no financial conflicts of interest.

References

Ashrafizadeh, M. (2024) Cell death mechanisms in human cancers: molecular pathways, therapy resistance and therapeutic perspective. *Journal of Cancer Biomoleculars and Therapeutics* **1**, 17-40.

Bogdan, A. R., Miyazawa, M., Hashimoto, K. et al. (2016) Regulators of iron homeostasis: new players in metabolism, cell death, and disease. *Trends Biochem. Sci*. **41**, 274-286.

Cazzanelli, P., Wuertz-Kozak, K. (2020) MicroRNAs in intervertebral disc degeneration, apoptosis, inflammation, and mechanobiology. *Int. J. Mol. Sci*. **21**, 3601.

Chen, J., Yang, X., Feng, Y. et al. (2022) Targeting ferroptosis holds potential for intervertebral disc degeneration therapy. *Cells* **11**, 3508.

Chen, X., Li, J., Kang, R. et al. (2021) Ferroptosis: machinery and regulation. *Autophagy* **17**, 2054-2081.

Cheung, K. M., Karppinen, J., Chan, D. et al. (2009) Prevalence and pattern of lumbar magnetic resonance imaging changes in a population study of one thousand forty-three individuals. *Spine (Phila Pa 1976)* **34**, 934-940.

Conrad, M., Kagan, V. E., Bayir, H. et al. (2018) Regulation of lipid peroxidation and ferroptosis in diverse species. *Genes Dev*. **32**, 602-619.

Cui, S., Liu, X., Liu, Y. et al. (2023) Autophagosomes defeat ferroptosis by decreasing generation and increasing discharge of free Fe^{2+} in skin repair cells to accelerate diabetic wound healing. *Adv. Sci. (Weinh.)* **10**, e2300414.

Dixon, S. J., Lemberg, K. M., Lamprecht, M. R. et al. (2012) Ferroptosis: an iron-dependent form of nonapoptotic cell death. *Cell* **149**, 1060-1072.

Dodson, M., Castro-Portuguez, R., Zhang, D. D. (2019) NRF2 plays a critical role in mitigating lipid peroxidation and ferroptosis. *Redox Biol*. **23**, 101107.

Doll, S., Proneth, B., Tyurina, Y. Y. et al. (2017) ACSL4 dictates ferroptosis sensitivity by shaping cellular lipid composition. *Nat. Chem. Biol*. **13**, 91-98.

Fratta Pasini, A. M., Stranieri, C., Busti, F. et al. (2023) New insights into the role of ferroptosis in cardiovascular diseases. *Cells* **12**, 867.

Fu, C., Wu, Y., Liu, S. et al. (2022) Rehmannioside A improves cognitive impairment and alleviates ferroptosis via activating PI3K/AKT/Nrf2 and SLC7A11/GPX4 signaling pathway after ischemia. *J. Ethnopharmacol*. **289**, 115021.

Galaris, D., Barbouti, A., Pantopoulos, K. (2019) Iron homeostasis and oxidative stress: an intimate relationship. *Biochim. Biophys. Acta Mol. Cell Res*. **1866**, 118535.

Han, C., Liu, Y., Dai, R. et al. (2020) Ferroptosis and its potential role in human diseases. *Front. Pharmacol*. **11**, 239.

Hashemi Goradel, N., Najafi, M., Salehi, E. et al. (2019) Cyclooxygenase-2 in cancer: a review. *J. Cell. Physiol*. **234**, 5683-5699.

Huang, Q., Sha, W., Gu, Q. et al. (2023) Inhibition of connexin43 improves the recovery of spinal cord injury against ferroptosis via the SLC7A11/GPX4 pathway. *Neuroscience* **526**, 121-134.

Jia, S., Yang, T., Gao, S. et al. (2024) Exosomes from umbilical cord mesenchymal stem cells ameliorate intervertebral disc degeneration via repairing mitochondrial dysfunction. *J. Orthop. Translat*. **46**, 103-115.

Jiang, X., Stockwell, B. R., Conrad, M. (2021) Ferroptosis: mechanisms, biology and role in disease. *Nat. Rev. Mol. Cell Biol*. **22**, 266-282.

Jin, Y., Qiu, J., Lu, X. et al. (2023) LncRNA CACNA1G-AS1 up-regulates FTH1 to inhibit ferroptosis and promote malignant phenotypes in ovarian cancer cells. *Oncol. Res*. **31**, 169-179.

Koppula, P., Zhang, Y., Zhuang, L. et al. (2018) Amino acid transporter SLC7A11/xCT at the crossroads of regulating redox homeostasis and nutrient dependency of cancer. *Cancer Commun. (Lond.)* **38**, 12.

Krut, Z., Pelled, G., Gazit, D. et al. (2021) Stem cells and exosomes: new therapies for intervertebral disc degeneration. *Cells* **10**, 2241.

Li, Y., Pan, D., Wang, X. et al. (2022) Silencing ATF3 might delay TBHP-induced intervertebral disc degeneration by repressing NPC ferroptosis, apoptosis, and ECM degradation. *Oxid. Med. Cell. Longev*. **2022**, 4235126.

Li, Z., Yu, X., Shen, J. et al. (2015) MicroRNA in intervertebral disc degeneration. *Cell Prolif*. **48**, 278-283.

Liu, H., Huang, X., Liu, X. et al. (2014) miR-21 promotes human nucleus pulposus cell proliferation through PTEN/AKT signaling. *Int. J. Mol. Sci*. **15**, 4007-4018.

Liu, W., Chakraborty, B., Safi, R. et al. (2021) Dysregulated cholesterol homeostasis results in resistance to ferroptosis increasing tumorigenicity and metastasis in cancer. *Nat. Commun*. **12**, 5103.

Liu, X., Zhong, S., Qiu, K. et al. (2023) Targeting NRF2 uncovered an intrinsic susceptibility of acute myeloid leukemia cells to ferroptosis. *Exp. Hematol. Oncol*. **12**, 47.

Lu, S., Song, Y., Luo, R. et al. (2021) Ferroportin-dependent iron homeostasis protects against oxidative stress-induced nucleus pulposus cell ferroptosis and ameliorates intervertebral disc degeneration in vivo. *Oxid. Med. Cell. Longev*. **2021**, 6670497.

Lu, Z., Zheng, Z. (2023) Integrated analysis of single-cell and bulk RNA sequencing data identifies the characteristics of ferroptosis in lumbar disc herniation. *Funct. Integr. Genomics* **23**, 289.

Nishizawa, H., Matsumoto, M., Shindo, T. et al. (2020) Ferroptosis is controlled by the coordinated transcriptional regulation of glutathione and labile iron metabolism by the transcription factor BACH1. *J. Biol. Chem*. **295**, 69-82.

Salatino, A., Aversa, I., Battaglia, A. M. et al. (2019) H-Ferritin affects cisplatin-induced cytotoxicity in ovarian cancer cells through the modulation of ROS. *Oxid. Med. Cell. Longev*. **2019**, 3461251.

Sun, Y., Zhang, W. Li, X. (2021) Induced pluripotent stem cell-derived mesenchymal stem cells deliver exogenous miR-105-5p via small extracellular vesicles to rejuvenate senescent nucleus pulposus cells and attenuate intervertebral disc degeneration. *Stem Cell Res. Ther*. **12**, 286.

Tsirimonaki, E., Fedonidis, C., Pneumaticos, S. G. et al. (2013) PKCε signalling activates ERK1/2, and regulates aggrecan, ADAMTS5, and miR377 gene expression in human nucleus pulposus cells. *PLoS One* **8**, e82045.

Wu, X., Li, Y., Zhang, S. et al. (2021) Ferroptosis as a novel therapeutic target for cardiovascular disease. *Theranostics* **11**, 3052-3059.

Xin, J., Wang, Y., Zheng, Z. et al. (2022) Treatment of intervertebral disc degeneration. *Orthop. Surg*. **14**, 1271-1280.

Yang, F., Wang, J., Chen, Z. et al. (2021a) Role of microRNAs in intervertebral disc degeneration (Review). *Exp. Ther. Med*. **22**, 860.

Yang, R. Z., Xu, W. N., Zheng, H. L. et al. (2021b) Involvement of oxidative stress-induced annulus fibrosus cell and nucleus pulposus cell ferroptosis in intervertebral disc degeneration pathogenesis. *J. Cell. Physiol*. **236**, 2725-2739.

Yu, Y., Yan, Y., Niu, F. et al. (2021) Ferroptosis: a cell death connecting oxidative stress, inflammation and cardiovascular diseases. *Cell Death Discov*. **7**, 193.

Yuan, H., Li, X., Zhang, X. et al. (2016) Identification of ACSL4 as a biomarker and contributor of ferroptosis. *Biochem. Biophys. Res. Commun*. **478**, 1338-1343.

Zeng, C., Lin, J., Zhang, K. et al. (2022) SHARPIN promotes cell proliferation of cholangiocarcinoma and inhibits ferroptosis via p53/SLC7A11/GPX4 signaling. *Cancer Sci*. **113**, 3766-3775.

Zhang, F., Zhao, X., Shen, H. et al. (2016) Molecular mechanisms of cell death in intervertebral disc degeneration (Review). *Int. J. Mol. Med*. **37**, 1439-1448.

Zhang, J., Liu, R., Mo, L. et al. (2023) miR-4478 accelerates nucleus pulposus cells apoptosis induced by oxidative stress by targeting MTH1. *Spine (Phila Pa 1976)* **48**, E54-E69.

Zhang, Y., Han, S., Kong, M. et al. (2021) Single-cell RNA-seq analysis identifies unique chondrocyte subsets and reveals involvement of ferroptosis in human intervertebral disc degeneration. *Osteoarthritis Cartilage* **29**, 1324-1334.

Zielinska, N., Podgórski, M., Haładaj, R. et al. (2021) Risk factors of intervertebral disc pathology – a point of view formerly and today - a review. *J. Clin. Med*. **10**, 409.